Kinetics of the Gas-Phase O(1 D) + CO 2 and C(1 D) + CO 2 Reactions over the 50–296 K Range

Dianailys Nuñez-Reyes, Kevin Hickson

Kinetics of the Gas-Phase $O(^1D) + CO_2$ and $C(^1D) + CO_2$ Reactions Over the 50 - 296 K Range

Dianailys Nuñez-Reyes[a,b] and Kevin M. Hickson,*[,a,b]

[a]*Université de Bordeaux, Institut des Sciences Moléculaires, F-33400 Talence, France*

[b]*CNRS, Institut des Sciences Moléculaires, F-33400 Talence, France*

Abstract: The kinetics of the reactions of CO_2 with atomic oxygen and atomic carbon in their first excited singlet states have been studied at room temperature and below using the Laval nozzle reactor method. $O(^1D)$ and $C(^1D)$ atoms were created in-situ by the 266 nm pulsed laser photolysis of O_3 and CBr_4 precursor molecules respectively. While $O(^1D)$ atoms were detected directly by vacuum ultra violet laser induced fluorescence at 115 nm, $C(^1D)$ atoms were followed indirectly through a chemical tracer method. The measured rate constants for the $O(^1D) + CO_2$ reaction are found to be in excellent agreement with earlier work and extend the available kinetic data for this process down to 50 K. The present work represents the first kinetics study of the $C(^1D) + CO_2$ reaction below room temperature. Both reactions display rate constants that increase as the temperature falls, with a more substantial rate increase observed for the $O(^1D) + CO_2$ reaction. This finding could be due to the increasing lifetimes of the intermediate species involved at lower temperatures.

1 Introduction

Neutral 'radical' atoms are considered to play important roles in the chemistry of a range of astrophysical environments[1]. In particular, the reactions of ground state atoms $C(^3P)$, $N(^4S)$ and $O(^3P)$ with cations such as H_3^+ are important processes in the formation of neutral hydrides[2]

and other reactions with small molecules and molecular radicals lead to an overall increase in the chemical complexity of dense interstellar clouds.[3,4] Although reactions involving atoms in excited electronic states C(^{1}D), N(^{2}D) and O(^{1}D) are unlikely to contribute to the gas-phase chemistry of the interstellar medium given the short radiative lifetimes of these species and the low molecular densities involved, there is evidence to suggest that these processes could occur in interstellar ices, leading to complex organic molecule formation.[5,6] In planetary atmospheres, the short wavelength photodissociation of simple molecules such as O_2, CO and N_2 generates neutral atoms in both the ground and excited electronic states. As the atmospheric densities are many orders of magnitude higher than those found in the interstellar medium, excited state atoms make important contributions to the overall gas-phase chemistry. In these environments, the reactive removal of excited state atoms competes with non-reactive quenching losses that lead to ground state atom formation.

In the Martian atmosphere, O(^{1}D) atoms are produced with high quantum yields by the photodissociation of CO_2 below 170 nm.[7] Similarly, the photodissociation of CO molecules below 100 nm has been shown to produce significant quantities of C(^{1}D) atoms[8] which could also play a small role in Mars atmospheric chemistry. Indeed, both CO_2 and CO possess highly structured absorption features in the 90 - 100 nm range so that CO might not be entirely shielded by CO_2 in this spectral region. To quantify the importance of excited state atoms to the chemistry requires an accurate knowledge of the rate constants for the most important reactive and non-reactive removal processes in any particular environment. In the case of O(^{1}D), these atoms will either react with species present in the Martian atmosphere such as H_2 or H_2O or be removed by non-reactive collisions with the major atmospheric constituent CO_2 (95 %) through the formation of an intermediate CO_3 species.[9] Rate constants have been measured for this process over a combined range of temperatures 139 K - 673 K in three separate studies[10-12] in addition to measurements at room temperature.[13-17] These earlier studies clearly show that the

quenching rate is large and increases further as the temperature falls, reaching a value of (1.2 ± 0.1) × 10^{-10} cm^3 s^{-1} at 139 K.

In contrast to the O(^{1}D) + CO_2 reaction, the removal of C(^{1}D) atoms by CO_2 is considered to be a reactive process leading adiabatically over the ^{1}A' potential energy surface (in C_s symmetry) to yield two CO molecules in the ground electronic $^1\Sigma^+$ state with an exothermicity of approximately 420 kJ mol^{-1}.[18] The only previous experimental kinetic study of this process was performed at room temperature yielding a value of (3.7 ± 1.7) × 10^{-11} cm^3 s^{-1} for the rate constant.[19]

Here we report the results of an experimental investigation of the O(^{1}D) + CO_2 and C(^{1}D) + CO_2 reactions in the gas-phase over the 50 - 296 K temperature range using a Laval nozzle reactor coupled with pulsed laser photolysis to generate O(^{1}D) and C(^{1}D) atoms. To examine the reaction kinetics, O(^{1}D) atoms were probed directly by vacuum ultraviolet laser induced fluorescence whereas C(^{1}D) atoms were followed indirectly using a chemical tracer method. Section 2 describes the experimental methods used to perform this study and the results obtained are discussed in section 3. The conclusions are presented in Section 4.

2 Experimental Methods

The experiments reported here were carried out using a supersonic flow reactor[20] operating in continuous mode. The apparatus has been described in detail in our earliest publications,[21,22] with further modifications that allowed the kinetics of atom + molecule reactions to be investigated reported in more recent work.[23-36] The key element of this instrument is the axisymmetric Laval nozzle, allowing uniform supersonic flows with a known low temperature to be generated through the isentropic expansion of a specified carrier gas into a vacuum chamber. In these experiments, argon was exclusively used as the carrier gas due to the fast electronic quenching of both O(^{1}D) and C(^{1}D) atoms by other potential carrier gases such as N_2.[26,30] Supersonic flows with characteristic temperatures of 50 K, 75 K and 127 K could be

created using three different Ar based Laval nozzles with the calculated and measured properties presented in Table 1. To extend the temperature range of the experiments to 296 K, measurements were also performed without a nozzle, effectively using the apparatus as a conventional slow-flow flash photolysis system.

Table 1 Characteristics of the supersonic flows

Mach number	2.0 ± 0.03[a]	3.0 ± 0.1	3.9 ± 0.1
Carrier gas	Ar	Ar	Ar
Density ($\times 10^{16}$ cm^{-3})	12.6 ± 0.3	14.7 ± 0.6	25.9 ± 0.9
Impact pressure (Torr)	10.5 ± 0.2	15.3 ± 0.5	29.6 ± 1.0
Stagnation pressure (Torr)	13.9	34.9	113
Temperature (K)	127 ± 2	75 ± 2	50 ± 1
Mean flow velocity (ms^{-1})	419 ± 3	479 ± 3	505 ± 1
Chamber pressure (Torr)	1.5	1.2	1.4

[a] The errors on the Match number, density, temperature and mean flow velocity (1σ) are calculated from separate measurements of the impact pressure using a Pitot tube as a function of distance from the Laval nozzle and the stagnation pressure within the reservoir.

For the study of the $O(^1D) + CO_2$ reaction, $O(^1D)$ atoms were created in situ in the cold flow by the 10 Hz pulsed laser photolysis of ozone (O_3) at 266 nm with an energy of ~23 mJ. This process is known to have a high quantum yield in the UV wavelength range.[37] Although $O(^3P)$ is also produced in low yields by the photolysis and as a quenching product, the $O(^3P) + CO_2$ reaction does not occur at these temperatures. Precursor O_3 molecules were generated upstream of the Laval nozzle through the termolecular $O(^3P) + O_2 + M(O_2)$ reaction in a separate cell maintained at pressures around 700 Torr. $O(^3P)$ atoms were produced by the continuous irradiation of O_2 in the cell by the UV output of a pen ray mercury lamp. O_3 concentrations were estimated to be in the range (5-7) $\times$ 10^{12} cm^{-3} assuming that 5% of the initial O_2 was photodissociated. $O(^1D)$ atoms were detected through resonant pulsed vacuum ultraviolet laser induced fluorescence (VUV LIF) at 115.215 nm via the $3s\ ^1D - 2p\ ^1D$ transition of $O(^1D)$. The

procedure to generate tunable light at this wavelength by frequency tripling has already been described in earlier work.[23,26,34,36]

For the study of the $C(^1D) + CO_2$ reaction, $C(^1D)$ atoms were produced through the multiphoton dissociation of carbon tetrabromide (CBr_4), which was introduced into the reactor by passing argon over solid CBr_4 held in a flask at a known pressure and temperature. CBr_4 concentrations in the range $(0.4 - 1.7) \times 10^{13}$ cm^{-3} were used in the present investigation.

The main atomic products of CBr_4 photolysis at 266 nm are $C(^3P)$ atoms[27] although these do not interfere as the $C(^3P) + CO_2(X^1\Sigma_g^+) \rightarrow CO(X^1\Sigma^+) + CO(X^1\Sigma^+)$ reaction is spin-forbidden and very slow at room temperature[18] while the formation of the spin-allowed products $CO(X^1\Sigma^+) + CO(a^3\Pi)$ is endothermic. CBr, CBr_2 and CBr_3 are also expected to be formed by the photodissociation of CBr_4. $C(^1D)$ atoms were not detected directly during this study due to the absence of strong electronic transitions in accessible wavelength ranges. To circumvent this problem, H_2 or CH_4 was added to the flow in a fixed low concentration. As both H_2 and CH_4 react rapidly with $C(^1D)$ atoms ($C(^3P)$ atoms are unreactive towards both H_2 and CH_4) to yield atomic hydrogen as major products,[24,33] it was possible to follow H-atom production by VUV LIF detection at 121.567 nm via the $1s\ ^2S \rightarrow 2p\ ^2P^0$ Lyman-α transition, effectively employing H-atoms to track the progress of the competing $C(^1D) + CO_2$ reaction. The kinetic analysis used is explained in more detail in the results section. The frequency tripling method used to produce tunable light around 121.567 nm has been well described in previous papers.[24,25,30,33,35]

The tripling cell was attached to the reactor at the level of the detection region by a 75 cm long sidearm containing baffles. This ensured that most of the divergent UV radiation from the tripling cell was eliminated before it reached the reactor and significantly reduced the level of the scattered light signal. For both studies, it was necessary to constantly flush the sidearm to prevent secondary absorption of the VUV radiation by residual gases. The VUV beam was directed into the reactor, at 90 degrees to both the cold supersonic flow and the detector. On

resonance VUV emission from excited state atoms within the flow was detected by a solar blind photomultiplier tube (PMT) which was protected from reactive gases within the chamber by a LiF window. The region between the LiF window and the PMT was evacuated, allowing the atomic fluorescence to reach the detector. This zone also contained a LiF lens to focus the VUV emission onto the photocathode of the PMT. The output of the PMT was connected to a boxcar integration system for processing. The fluorescence signal was averaged over 30 probe laser shots at any given time delay between the photolysis and probe lasers. At least 75 time points were acquired for any single decay profile with at least 15 time points recorded at negative delays to obtain the baseline level.

The gases used in the experiments (reactive gases, carrier gases, flush gases and rare gases for frequency tripling) were all controlled by digital mass flow controllers connected directly to the cylinders themselves. These devices were calibrated by recording the pressure rise brought about by flowing a specified gas into a known fixed volume. The suppliers and purities of the individual gases used are (Linde Ar 99.999%, O_2 99.999%, Kr 99.999% Xe 99.999%, CO_2 99.998%, CH_4 99.9995 %, Air Liquide N_2 99.999%, H_2 99.9999%).

3 Results and Discussion

Kinetics of the $O(^1D) + CO_2$ reaction

Excess concentrations of coreagent CO_2 were used for all experiments. Consequently, the pseudo-first-order approximation was assumed to be valid, so that a single exponential function of the form

$$I_{O(^1D)} = I_{O(^1D)_0} exp(-k't) \quad (1)$$

could be used to describe the variation of the $O(^1D)$ VUV LIF signal, $I_{O(^1D)}$, as a function of time between the photolysis and probe lasers. k' is the pseudo-first-order $O(^1D)$ loss rate and $I_{O(^1D)_0}$ is the $O(^1D)$ VUV LIF signal when time $t = 0$. In these experiments, k' has two major contributions; $k_{O(^1D) + Ar}[Ar] + k_{O(^1D) + CO_2}[CO_2]$ where $k_{O(^1D) + Ar}$ and $k_{O(^1D) + CO_2}$ are the

second-order rate constants for O(^{1}D) removal by Ar and CO_2 respectively. As $k_{O(^1D) + Ar}[Ar]$ is large due to the large carrier gas density, O(^{1}D) decays are seen to be rapid even in the absence of CO_2 as shown in Figure 1.

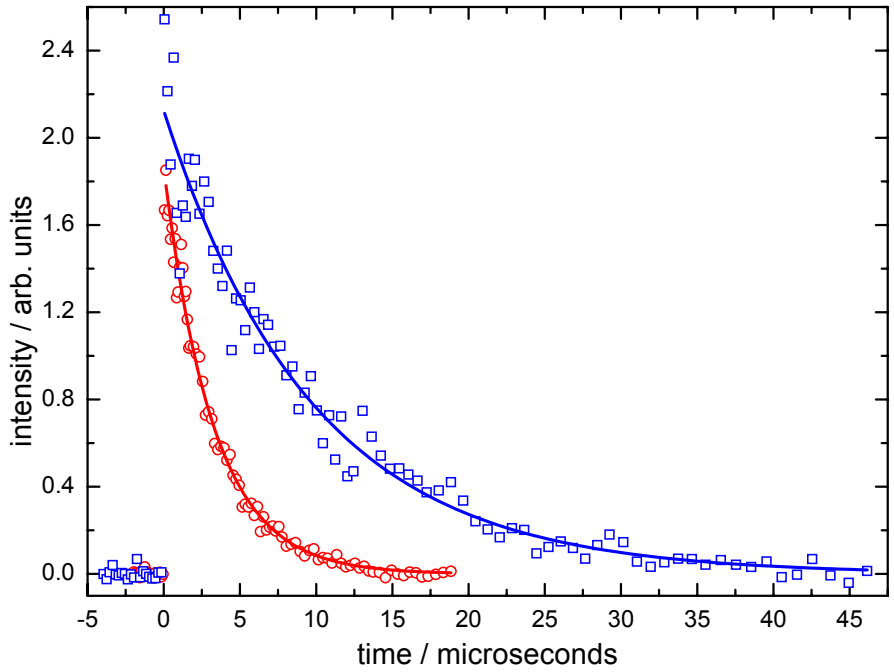

Figure 1 Variation of the O(^{1}D) VUV LIF signal as a function of time recorded at 296 K. (Red open circles) [CO_2] = 1.57 × 10^{15} cm^{-3}; (blue open squares) without CO_2 (O(^{1}D) decay due to non-reactive quenching collisions with the carrier gas argon).

Kinetics decays similar to those shown in Figure 1 were recorded for a range of [CO_2] allowing k' values to be derived from the fits. The k' values determined at any given temperature were plotted against the corresponding CO_2 concentration. A weighted linear least-squares fit to these data yielded $k_{O(^1D) + CO_2}$. Typical plots of this type obtained at 296 K and 50 K are shown in Figure 2 where the large y-axis intercept value of the straight-line plots results from quenching losses through O(^{1}D) collisions with the carrier gas Ar, $k_{O(^1D) + Ar}[Ar]$.

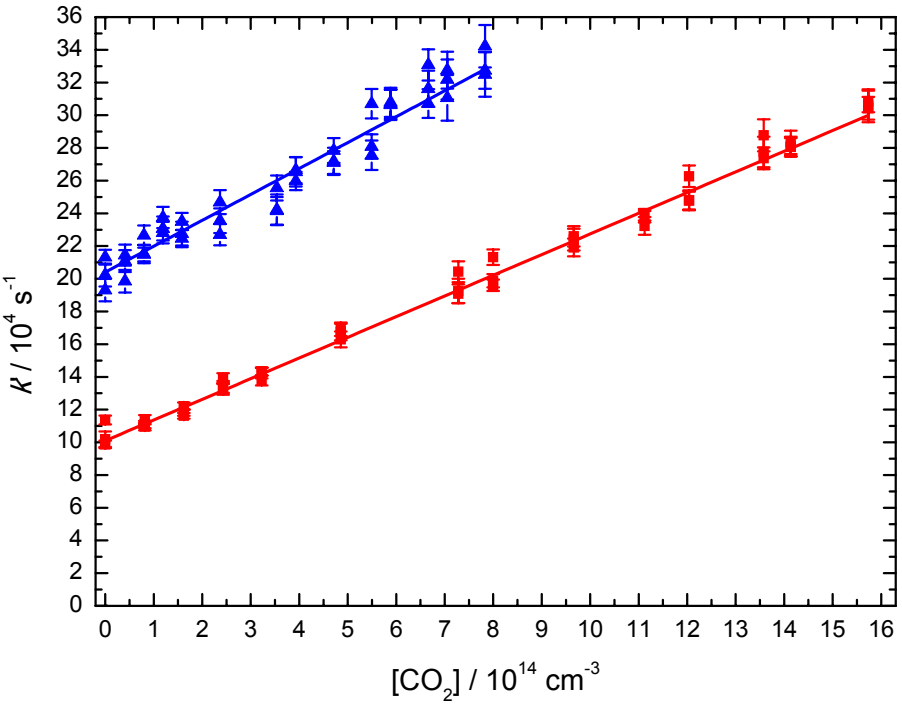

Figure 2 Measured pseudo-first-order rate constants for the $O(^1D) + CO_2$ reaction as a function of $[CO_2]$. (Red solid squares) data recorded at 296 K; (blue solid triangles) data recorded at 50 K. The solid red and blue lines represent linear least-squares fits to the datasets, weighted by the statistical uncertainties of the individual datapoints (obtained through exponential fits of expression (1) to curves similar to those shown in Figure 1).

The y-axis intercept is larger for measurements recorded at 50 K due to the higher Ar carrier gas density in these experiments ($[Ar] = 2.6 \times 10^{17}$ cm^{-3} at 50 K, whereas $[Ar] = 1.6 \times 10^{17}$ cm^{-3} at 296 K) while the $O(^1D)$ + Ar quenching rate constant increases slightly as the temperature falls.[26]

Figure 3 shows $k_{O(^1D) + CO_2}$ plotted as a function of temperature alongside earlier experimental and theoretical results. The measured rate constants are summarized in Table 2.

Table 2 Temperature dependent rate constants for the $O(^1D) + CO_2$ and $C(^1D) + CO_2$ reactions

T / K	N^b	$[CO_2]/10^{14}$ cm^{-3}	$k_{O(1D)+CO2}$ / cm^3 s^{-1}	N^b	$[CO_2]/10^{14}$ cm^{-3}	$k_{C(1D)+CO2}$ / cm^3 s^{-1}
296	42	0-15.7	$(1.3 \pm 0.1)^c \times 10^{-10}$	42	0-15.7	$(4.2 \pm 0.4)^c \times 10^{-11}$
127 ± 2^a	42	0-11.5	$(1.4 \pm 0.1) \times 10^{-10}$	41	0-11.6	$(4.6 \pm 0.5) \times 10^{-11}$
75 ± 2	42	0-5.7	$(1.5 \pm 0.2) \times 10^{-10}$	42	0-5.7	$(5.4 \pm 0.6) \times 10^{-11}$
50 ± 1	42	0-7.8	$(1.6 \pm 0.2) \times 10^{-10}$	42 18	0-2.4 0-2.4	$(5.8 \pm 0.8) \times 10^{-11}$ $(5.3 \pm 0.9) \times 10^{-11}$

[a]Uncertainties on the calculated temperatures represent the statistical (1σ) errors obtained from Pitot tube measurements of the impact pressure. [b]Number of individual measurements. [c]Uncertainties on the measured rate constants represent the combined statistical (1σ) and estimated systematic (10%) errors.

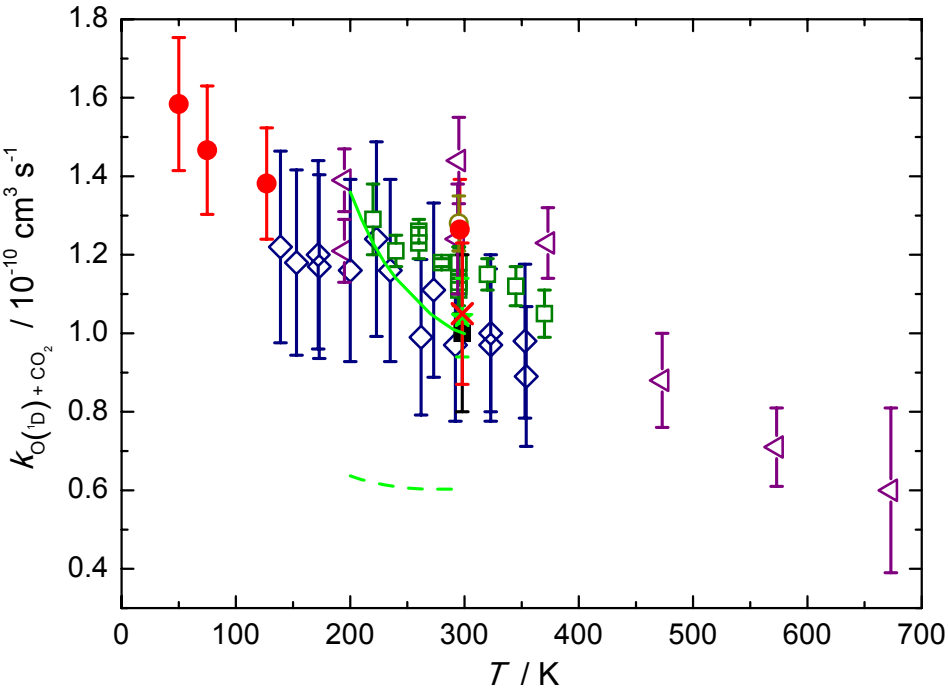

Figure 3 Temperature dependence of the rate constant for the $O(^1D)$ + CO_2 reaction. Experimental studies (solid red circles) this work; (open blue diamonds) Streit et al.[10]; (open purple triangles) Blitz et al.[12]; (open green squares) Dunlea and Ravishankara[11]; (open yellow circle) Amimoto et al.[17]; (solid black square) Davidson et al.[13]; (solid green star) Wine and Ravishankara[14]; (red cross) Shi and Barker.[16] Theoretical studies (dashed green line) Mebel et al.[9] using a TS energy of -1.26 kJ/mol; (solid green line) Mebel et al.[9] using a TS energy of -2.51 kJ/mol. Error bars on the present results represent the combined statistical (1σ) and systematic (10 %) uncertainties.

The error bars on these values contain contributions from both statistical and systematic uncertainties. Systematic errors, which are estimated to be around 10%, could have arisen from several sources including uncertainties in the calibration of the mass-flow controllers and the subsequent determinations of the concentrations of the reactants and the supersonic flow density as well as possible errors in pressure gauges and other instruments.

The measured rate constant at 296 K, $k_{O(^1D)+CO_2}(296\ K) = (1.3 \pm 0.1) \times 10^{-10}$ cm^3 s^{-1} is in excellent agreement with previous absolute determinations of the rate constant at room temperature[10-14,16,17] which are all in the range (1.0-1.4) × 10^{-10} cm^3 s^{-1} using a variety of direct and indirect methods to follow the progress of the reaction. In terms of the temperature dependence of the $O(^1D)$ + CO_2 reaction, there are three earlier experimental studies covering a combined temperature range of 139 - 673 K by Streit et al.,[10] Blitz et al.[12] and Dunlea et al.[11] These studies found that the rate constant increases with decreasing temperature, with all three datasets displaying similar dependences. The present results are seen to be entirely consistent with earlier work both in terms of the magnitude and temperature dependence of the derived rate constant values, and extend the available kinetic data down to 50 K.

Mebel and coworkers[9] used ab-initio multireference configuration interaction methods to provide more detail on the mechanism of the $O(^1D) + CO_2$ reaction and its kinetics. They calculated the geometries and energies of the various intermediates and transition states (TSs) over the lowest singlet and triplet potential energy surfaces of CO_3. They showed that reaction occurs through the formation of an initial $O\text{-}CO_2$ van de Waals complex which could then isomerize to form a strongly bound cyclic CO_3 intermediate over a submerged barrier on the singlet PES calculated to be 1.26 kJ/mol lower than the reagent asymptote as a best estimate. As the exit channel to form $CO + O_2$ products is thought to be characterized by a barrier,[38] loss of singlet CO_3 is dominated by quenching through intersystem crossing to the triplet CO_3 potential energy surface followed by dissociation to $O(^3P)$ and CO_2. Using standard RRKM theory[39] Mebel et al.[9] calculated rate constants for the various isomerization and dissociation steps on the singlet and triplet CO_3 PESs in addition to intersystem crossing rate constants and radiationless transitions between the triplet and singlet surfaces. This allowed the authors to derive the overall rate constant for the $O(^1D) + CO_2$ reaction as a function of temperature. These values are presented alongside the experimental ones in Figure 3 for two different energy values of the submerged barrier on the singlet CO_3 PES. It can be seen that the best estimate value of -1.26 kJ/mol for this transition state leads to calculated rate constants which are half as large as the experimental ones. The agreement is significantly improved however when a lower value of -2.51 kJ/mol is used instead. With regard to the derived temperature dependence of the reaction rate, Mebel et al.[9] found that this quantity was mostly dependent on the energy dependence of the unimolecular dissociation rate for the cyclic $^1CO_3$ intermediate. Indeed, the triplet state quenching products were found to be primarily formed through a radiationless transition from a planar $^1CO_3$ structure with D_{3h} symmetry to a $^3CO_3$ structure with C_{2v} symmetry, with only a weak dependence on the initial energy rather than through a minimum on the seam of crossing between singlet and triplet surfaces. Consequently, as the initial

collision energy (temperature) decreases, a slower redissociation rate for the cyclic $^1CO_3$ intermediate leads to an enhanced rate of formation of $O(^3P) + CO_2$ products.

Kinetics of the $C(^1D) + CO_2$ reaction

In a similar manner to the experiments on the $O(^1D) + CO_2$ reaction, The pseudo-first-order approximation was applied to investigate the kinetics of the $C(^1D) + CO_2$ reaction. In this case, CO_2 and H_2 (or CH_4) (used to trace the kinetics of $C(^1D)$ loss through the $C(^1D) + H_2 \rightarrow CH + H$ or $C(^1D) + CH_4 \rightarrow C_2H_3 + H$ / $C_2H_2 + H_2$ reactions) were maintained in excess with respect to $C(^1D)$ atoms, although only the CO_2 concentration was varied for any series of measurements. Under these conditions, the H-atom fluorescence signal was well described by a biexponential function of the form

$$I_H = A\{exp(-k'_L t) - exp(-k'_F t)\} \quad (2)$$

where k'_L and k'_F are the pseudo-first-order rate constants for H-atom loss and formation respectively and A is the amplitude of the H-atom fluorescence signal. In the absence of competing secondary reactions, k'_L represents the diffusional loss of atomic hydrogen from the probe volume. k'_F potentially contains contributions from several processes in the present experiments including

$$k'_F = \sum k_{C(^1D)+CO_2}[CO_2] + k_{C(^1D)+H_2(CH_4)}[H_2]([CH_4]) + k_{C(^1D)+CBr_4}[CBr_4] + k_{C(^1D)+Ar}[Ar] + k_{diff,C(^1D)} \quad (3)$$

where $k_{C(^1D)+X}$ represents the second-order rate constant for $C(^1D)$ removal with species X and $k_{diff,C(^1D)}$ is the first-order diffusional loss of $C(^1D)$ atoms. The last four terms in expression (3) are constant for any single series of measurements, so that k'_F varies only as a function of $[CO_2]$. Two typical temporal profiles are displayed in Figure 4, obtained at 296 K for high (1.57×10^{15} cm^{-3}) $[CO_2]$ and without $[CO_2]$.

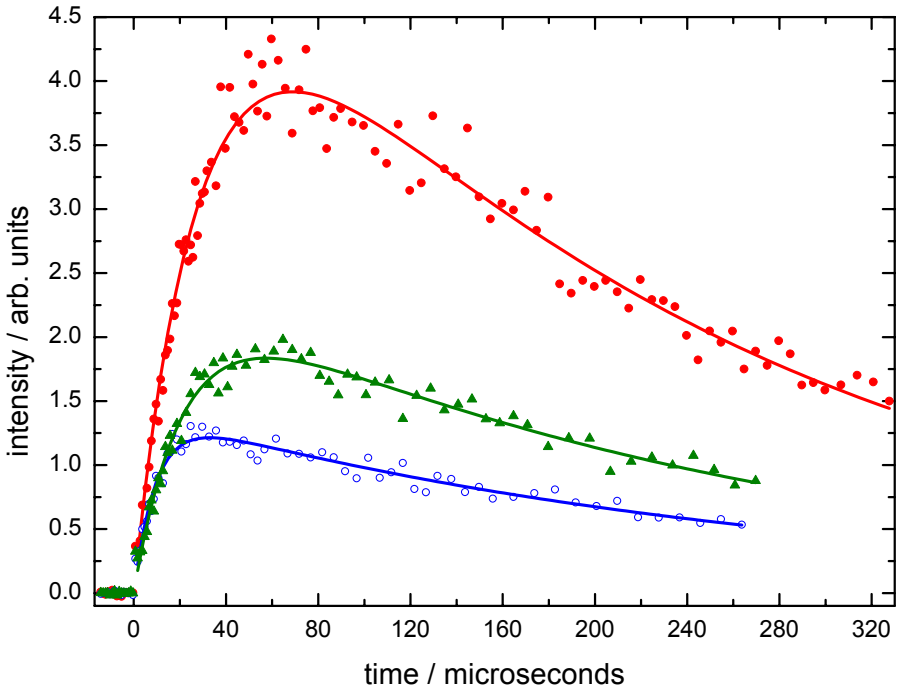

Figure 4 H-atom VUV LIF signal measured at 296 K as a function of time, effectively following the variation of the C(^{1}D) atom concentration through a chemical tracer method with [H_2] = 6.76 × 10^{13} cm^{-3}. (Red solid circles) without CO_2; (blue open circles) [CO_2] = 1.57 × 10^{15} cm^{-3}; (green solid triangles) [CO_2] = 3.17 × 10^{14} cm^{-3}.

Once the values of k'_F were extracted from biexponential fits to temporal profiles such as those shown in Figure 4, an identical procedure to the one used for the O(^{1}D) + CO_2 measurements was used to derive the temperature dependent second-order rate constants. Typical plots of the pseudo-first-order rate constant versus [CO_2] are presented in Figure 5 and the second-order rate constants are plotted as a function of temperature in Figure 6.

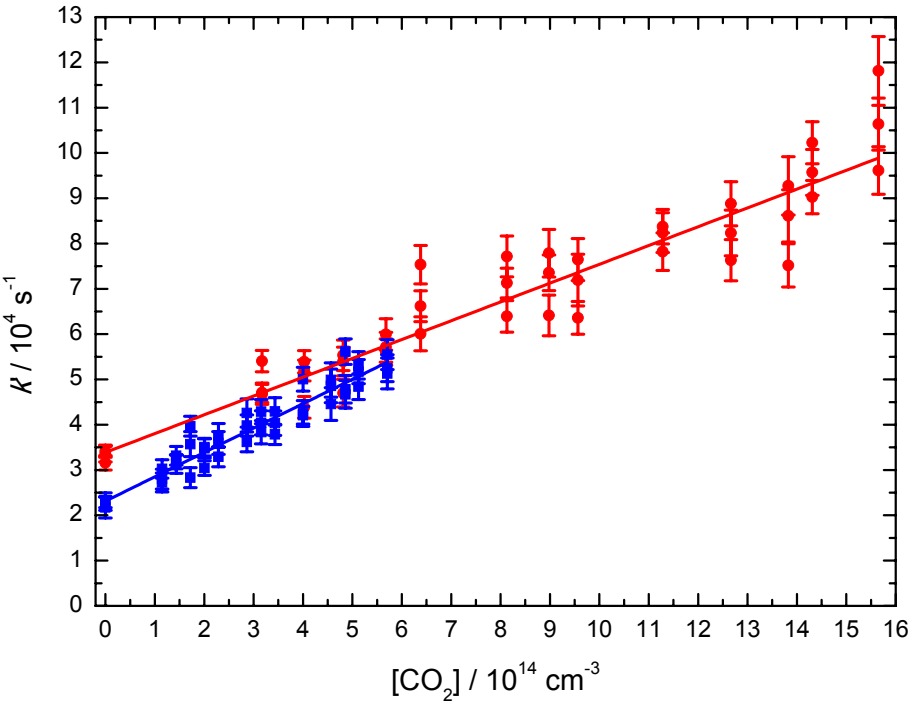

Figure 5 Measured pseudo-first-order rate constants for the $C(^1D) + CO_2$ reaction as a function of $[CO_2]$. (Red solid circles) data recorded at 296 K; (blue solid squares) data recorded at 75 K. The solid red and blue lines represent linear least-squares fits to the datasets, weighted by the statistical uncertainties of the individual datapoints (obtained through biexponential fits of expression (2) to curves similar to those shown in Figure 4).

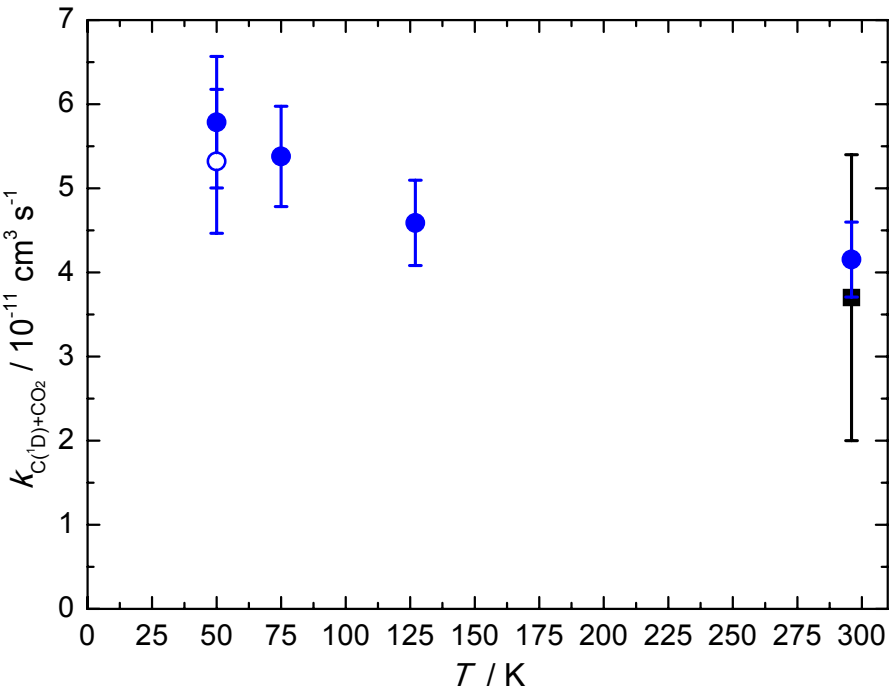

Figure 6 Temperature dependence of the rate constant for the C(^{1}D) + CO_2 reaction. (Black solid square) Husain and Kirsch[19]; (blue solid circles) this work using H_2 as the H-atom source; (blue open circle) this work using CH_4 as the H-atom source. Error bars on the present results represent the combined statistical (1σ) and systematic (10 %) uncertainties.

The y-axis intercept values of the second-order curves shown in Figure 5 correspond essentially to the terms $k_{C(^1D)+H_2}[H_2] + k_{C(^1D)+CBr_4}[CBr_4]$ (relaxation of C(^{1}D) by Ar is slow in this case). Values of [H_2] and [CBr_4] are chosen to provide good signal-to-noise levels for H-atom detection.

The rate constant measured in the present study at 296 K of (4.2 ± 0.4) × 10^{-11} cm^3 s^{-1} using H_2 as the H-atom source is in excellent agreement with the value obtained at 300 K by the only other previous investigation of this reaction by Husain and Kirsch[19] of (3.7 ± 1.7) × 10^{-11} cm^3 s^{-1}. These authors used the vacuum ultraviolet flash photolysis of carbon suboxide, C_3O_2, as the

source of C(^{1}D) atoms in their experiments, which were followed by time resolved atomic absorption spectroscopy. The present study represents the only measurements of the C(^{1}D) + CO_2 reaction below room temperature and clearly show that the rate constant increases as the temperature decreases reaching a value of (5.8 ± 0.8) × 10^{-11} cm^3 s^{-1} at 50 K. Supplementary measurements were performed at this temperature using CH_4 as the H-atom source, to check for possible effects of additional H-atom production induced by any subsequent reactions of highly reactive CH radicals produced in the C(^{1}D) + H_2 → CH + H reaction during the main experiments. In this instance, the measured rate constant ($k_{C(^1D)+CO_2}$ = (5.3 ± 0.9) × 10^{-11} cm^3 s^{-1}) is seen to be very similar to the one obtained using H_2 as the H-atom source. While this observation does not entirely rule out potential interferences from secondary chemistry, such processes are likely to play only a minor role in the present experiments.

The reaction of C(^{1}D) with CO_2 is expected to occur through the insertion of C(^{1}D) into one of the C=O bonds of CO_2, forming a transient ethylenedione molecule in an excited singlet state $^1C_2O_2$. According to previous theoretical work on the OCCO molecule,[40,41] the likely products of the C(^{1}D) + CO_2 reaction are two CO molecules in the ground $^1\Sigma^+$ state as the $^1C_2O_2$ intermediate is highly unstable. The formation of CO($X^1\Sigma^+$) + CO($a^3\Pi$) through a non-adiabatic transition to the $^3\Sigma_g^-$ state of C_2O_2 is not possible in this instance as these products are approximately 160 kJ mol^{-1} above the reagent level. One other possible outcome of the reaction is quenching to form ground state C(^{3}P) atoms and CO_2 in a quenching pathway. Nevertheless, as these products are higher in energy than the crossing point of the $^3\Sigma_g^-$ and $^1\Delta_g$ surfaces of the OCCO molecule according to the calculations of Schroder et al. (-122 kJ mol^{-1} for the former and -134 kJ mol^{-1} for the latter), the more likely outcome is CO($^1\Sigma^+$) formation from the ^{1}OCCO intermediate species. Other potential products such as C_2 + O_2 are also highly endothermic and should therefore be unimportant in the present experiments.

4 Conclusions

This work presents an experimental investigation of the temperature dependent kinetics of the reactions of oxygen and carbon atoms in the first excited singlet states with carbon dioxide. A supersonic (Laval nozzle) flow reactor was used to perform measurements of the rate constants for these processes at temperatures as low as 50 K. $O(^1D)$ and $C(^1D)$ atoms were generated directly in the supersonic flow through the pulsed laser photolysis of suitable precursor molecules introduced in low concentrations. $O(^1D)$ atoms were detected directly by vacuum ultraviolet laser induced fluorescence. In contrast, $C(^1D)$ atoms were followed indirectly through a chemical tracer method, using the $C(^1D) + H_2$ or CH_4 reactions as a source of atomic hydrogen which was followed by vacuum ultraviolet laser induced fluorescence. The derived rate constants for the $O(^1D) + CO_2$ quenching reaction are in excellent agreement with earlier work at higher temperature, displaying a negative temperature dependence over the entire range. The measured rate constants for the $C^1D) + CO_2$ reaction are in excellent agreement with the only other study of this process at room temperature. The reaction rate is seen to increase by almost 50 % as the temperature falls to 50 K.

AUTHOR INFORMATION

Corresponding Author

* Correspondence to: kevin.hickson@u-bordeaux.fr. Tel: +33 (0)5 40 00 63 42

Author Contributions

The manuscript was written through contributions of all authors. All authors have given approval to the final version of the manuscript.

Acknowledgement

K.M.H. and D.N.R acknowledge support from the French program ‘‘Physique et Chimie du Milieu Interstellaire” (PCMI) of the CNRS/INSU with the INC/INP co-funded by the CEA and CNES.

References

1. Sabbah, H.; Biennier, L.; Sims, I. R.; Georgievskii, Y.; Klippenstein, S. J.; Smith, I. W. M. Understanding Reactivity at Very Low Temperatures: The Reactions of Oxygen Atoms with Alkenes, *Science.* **2007**, *317*, 102–105.

2. Agundez, M.; Wakelam, V. Chemistry of Dark Clouds: Databases, Networks, and Models, *Chem. Rev.* **2013**, *113*, 8710-8737.

3. Loison, J.-C.; Hu, X.; Han, S.; Hickson, K. M.; Guo, H.; Xie, D. An Experimental and Theoretical Investigation of the $N(^4S) + C_2(^1\Sigma_g^+)$ Reaction at Low Temperature, *Phys. Chem. Chem. Phys.,* **2014**, *16*, 14212-14219.

4. Daranlot, J.; Hu, X.; Xie, C.; Loison, J.-C.; Caubet, P.; Costes, M.; Wakelam, V.; Xie, D.; Guo H.; Hickson, K. M. Low Temperature Rate Constants for the $N(^4S) + CH(X^2\Pi_r)$ Reaction. Implications for N_2 Formation Cycles in Dense Interstellar Clouds, *Phys. Chem. Chem. Phys.,* **2013**, *15*, 13888-13896.

5. Bergner, J. B.; Öberg K. I.; Rajappan, M. Methanol Formation via Oxygen Insertion Chemistry in Ices, *Astrophys. J.* **2017**, *845*, 29.

6. Herbst, E.; Dishoeck, E. F. Van. Complex Organic Interstellar Molecules, *Annu. Rev. Astron. Astrophys.,* **2009**, *47*, 427–480.

7. Schmidt, J. A.; Johnson M. S.; Schinke, R. Carbon Dioxide Photolysis from 150 to 210 nm: Singlet and Triplet Channel Dynamics, UV-spectrum, and Isotope Effects, *Proc. Natl. Acad. Sci. USA*, **2013**, *110*, 17691-17696.

8. Gao, H.; Song, Y.; Chang, Y.-C.; Shi, X.; Yin, Q.-Z.; Wiens, R. C.; Jackson, W. M.; Ng, C. Y. Branching Ratio Measurements for Vacuum Ultraviolet Photodissociation of $^{12}C^{16}O$, *J. Phys. Chem. A* 2013, *117*, 6185-6195.

9. Mebel, A. M.; Hayashi, M.; Kislov V. V.; Lin, S. H. Theoretical Study of Oxygen Isotope Exchange and Quenching in the $O(^1D) + CO_2$ Reaction, *J. Phys. Chem. A* **2004**, *108*, 7983-7994.

10. Streit, G. E.; Howard, C. J.; Schmeltekopf, A. L.; Davidson, J. A.; Schiff, H. I. Temperature-Dependence of $O(^1D)$ Rate Constants for Reactions with O_2, N_2, CO_2, O_3, and H_2O. *J. Chem. Phys.* **1976**, *65*, 4761−4764.

11. Dunlea, E. J.; Ravishankara, A. R. Kinetic Studies of the Reactions of $O(^1D)$ with Several Atmospheric Molecules. *Phys. Chem. Chem. Phys*. **2004**, *6*, 2152-2161.

12. Blitz, M. A.; Dillon, T. J.; Heard, D. E.; Pilling, M. J.; Trought, I. D. Laser Induced Fluorescence Studies of the Reactions of $O(^1D_2)$ with N_2, O_2, N_2O, CH_4, H_2, CO_2, Ar, Kr and n-C_4H_{10}. *Phys. Chem. Chem. Phys*. **2004**, *6*, 2162-2171.

13. Davidson, J. A.; Schiff, H. I. Streit, G. E.; McAfee, J. R.; Schmeltekopf, A. L.; Howard, C. J. Temperature dependence of $O(^1D)$ Rate Constants for Reactions with N_2O, H_2, CH_4, HCl, and NH_3. *J. Chem. Phys.* **1977**, *67*, 5021−5025.

14. Wine, P.H.; Ravishankara, A.R. Kinetics of $O(^1D)$ Interactions with the Atmospheric Gases N_2, N_2O, H_2O, H_2, CO_2, and O_3, *Chem. Phys. Lett*., **1981**, *77*, 103-109.

15. Young, R.A.; Black, G.; Slanger, T.G. Reaction and Deactivation of $O(^1D)$, *J. Chem. Phys*., **1968**, *49*, 4758-47689.

16. Shi, J.; Barker, J.R. Kinetic Studies of the Deactivation of $O_2(^1\Sigma_g^+)$ and $O(^1D)$, *Int. J. Chem. Kinet*., **1990**, *22*, 1283-1301.

17. Amimoto, S. T.; Force, A. P.; Gulotty, R. G.; Wiesenfeld, J. R. Collisional Deactivation of $O(2^1D_2)$ by the Atmospheric Gases. *J. Chem. Phys.* **1979,** *71*, 3640-3647.

18. Husain, D.; Newton, D. P. Collisional Quenching of Electronically Excited Carbon Atoms, $C[2p^2(^1S_0)]$, *J. Chem. Soc. Faraday Trans*. *2*, **1982**, *78*, 51-71.

19. Husain, D.; Kirsch, L. J. Study of Electronically Excited Carbon Atoms, $C(2^1D_2)$, by Time-resolved Atomic Absorption at 193.1 nm, $(3^1P_1^\circ \leftarrow 2^1D_2)$. Part 2. Reactions of $C(2^1D_2)$ with Molecules, *Trans*. *Faraday Soc.,* **1971**, *67*, 3166-3175.

20. Smith, I. W. M.; Rowe, B. R. Reaction Kinetics at Very Low Temperatures: Laboratory Studies and Interstellar Chemistry*, Accounts Chem. Res.,* **2000**, *33*, 261–268.

21. Daugey, N.; Caubet, P.; Retail, B.; Costes, M.; Bergeat, A.; Dorthe, G. Kinetic Measurements on Methylidyne Radical Reactions with Several Hydrocarbons at Low Temperatures. *Phys. Chem. Chem. Phys.* **2005,** *7*, 2921-2927.

22. Daugey, N.; Caubet, P.; Bergeat, A.; Costes M.; Hickson, K. M. Reaction Kinetics to Low Temperatures. Dicarbon + Acetylene, Methylacetylene, Allene and Propene from $77 \leq T \leq 296$ K. *Phys. Chem. Chem. Phys.* **2008**, *10*, 729-737.

23. Hickson, K. M.; Suleimanov, Y. V. Low-Temperature Experimental and Theoretical Rate Constants for the $O(^1D) + H_2$ Reaction. *J. Phys. Chem. A* **2017**, *121*, 1916-1923.

24. Hickson, K. M.; Loison, J.-C.; Guo H.; Suleimanov, Y. V. Ring-Polymer Molecular Dynamics for the Prediction of Low-Temperature Rates: An Investigation of the $C(^1D) + H_2$ Reaction. *J. Phys. Chem. Lett.* **2015**, *6*, 4194-4199.

25. Hickson, K. M.; Suleimanov, Y. V. An Experimental and Theoretical Investigation of the $C(^1D) + D_2$ Reaction. *Phys. Chem. Chem. Phys.* **2017**, *19*, 480-486.

26. Grondin, R.; Loison J.-C.; Hickson, K. M. Low Temperature Rate Constants for the Reactions of $O(^1D)$ with N_2, O_2 and Ar, *J. Phys. Chem. A,* **2016**, *120*, 4838-4844.

27. Shannon, R. J.; Cossou, C.; Loison, J.-C.; Caubet, P.; Balucani, N.; Seakins, P. W.; Wakelam, V.; Hickson, K. M. The Fast $C(^3P)$ + CH_3OH Reaction as an Efficient Loss Process for Gas-Phase Interstellar Methanol. *RSC Adv.* **2014**, *4*, 26342-26353.

28. Bourgalais, J.; Capron, M.; Kailasanathan, R. K. A.; Osborn, D. L.; Hickson, K. M.; Loison, J.-C.; Wakelam, V.; Goulay, F.; Le Picard, S. D., The $C(^3P)$ + NH_3 Reaction in Interstellar Chemistry. I. Investigation of the Product Formation Channels. *Astrophys. J.* **2015**, *812*, 106.

29. Hickson, K. M.; Loison, J.-C.; Bourgalais, J.; Capron, M.; Le Picard, S. D.; Goulay, F.; Wakelam, V. The $C(^3P)$ + NH_3 Reaction in Interstellar Chemistry. II. Low Temperature Rate Constants and Modeling of NH, NH_2, and NH_3 Abundances in Dense Interstellar Clouds. *Astrophys. J.* **2015**, *812*, 107.

30. Hickson, K. M.; Loison, J.-C.; Lique F.; Kłos, J. An Experimental and Theoretical Investigation of the $C(^1D)$ + N_2 → $C(^3P)$ + N_2 Quenching Reaction at Low Temperature. *J. Phys. Chem. A* **2016**, *120*, 2504-2513.

31. Hickson, K. M.; Loison, J.-C.; Nuñez-Reyes, D.; Méreau, R. Quantum Tunneling Enhancement of the C + H_2O and C + D_2O Reactions at Low Temperature. *J. Phys. Chem. Lett.* **2016**, *7*, 3641-3646.

32. Hickson, K. M.; Loison, J.-C.; Wakelam, V. Temperature Dependent Product Yields for the Spin Forbidden Singlet Channel of the $C(^3P)$ + C_2H_2 Reaction. *Chem. Phys. Lett.* **2016**, *659*, 70-75.

33. Nuñez-Reyes D.; Hickson, K. M. Kinetic and Product Study of the Reactions of $C(^1D)$ with CH_4 and C_2H_6 at Low Temperature. *J. Phys. Chem. A* **2017**, *121,* 3851-3857.

34. Meng, Q. Y.; Hickson, K. M.; Shao, K. J.; Loison, J.-C.; Zhang, D. H. Theoretical and Experimental Investigations of Rate Coefficients of $O(^1D) + CH_4$ at Low Temperature. *Phys. Chem. Chem. Phys.* **2016**, *18*, 29286-29292.

35. Nuñez-Reyes D.; Hickson, K. M. The Reactivity of $C(^1D)$ with Oxygen Bearing Molecules NO and O_2 at Low Temperature. *Chem. Phys. Lett.* **2017**, *687,* 330-335.

36. Nuñez-Reyes D.; Hickson, K. M.; Larrégaray, P.; Bonnet, L.; González-Lezana, T.; Suleimanov, Y. V. A Combined Theoretical and Experimental Investigation of the Kinetics and Dynamics of the $O(^1D) + D_2$ Reaction at Low Temperature. *Phys. Chem. Chem. Phys.* **2018**, *20*, 4404-4414.

37. Sander, S. P.; Abbatt, J.; Barker, J. R.; Burkholder, J. B.; Friedl, R. R.; Golden, D. M.; Huie, R. E.; Kolb, C. E.; Kurylo, M. J.; Moortgat, G. K.; Orkin, V. L.; Wine, P. H. Chemical Kinetics and Photochemical Data for Use in Atmospheric Studies, Evaluation No. 17. *JPL Publication 10-6, Jet Propulsion Laboratory, Pasadena, 2011* http://jpldataeval.jpl.nasa.gov/. **2011**.

38. Sedlacek, A. J.; Harding, D. R.; Weston Jr., R. E.; Kreutz, T. G.; Flynn, G. W. Probing the $O(^1D) + CO_2$ Reaction with Second-Derivative Modulated Diode Laser Spectroscopy. *J. Chem. Phys.* **1989**, *91*, 7550-7556.

39. Eyring, H.; Lin, S. H.; Lin, S. M. *Basic Chemical Kinetics*; Wiley: New York, 1980.

40. Talbi, D.; Chandler, G. S. Extensive ab Initio Study of the C_2O_2, C_2S_2, and C_2O_S Systems: Stabilities and Singlet-Triplet Energy Gaps. *J. Phys. Chem. A* **2000**, *104*, 5872-5881.

41. Schröder, D.; Heinemann, C.; Schwarz, H.; Harvey, J. N.; Dua, S.; Blanksby, S. J.; Bowie, J. H. Ethylenedione: An Intrinsically Short-Lived Molecule. *Chem. Eur. J.* **1998**, *4*, 2550-2557.